Optical model potentials for the ^{6}He + ^{209}Bi reaction from a ^{208}Pb(^{7}Li,^{6}He)^{209}Bi reaction analysis

L. Yang, C. J. Lin,* H. M. Jia, F. Yang, Z. D. Wu, X. X. Xu, H. Q. Zhang, Z. H. Liu, P. F. Bao, L. J. Sun, and N. R. Ma
China Institute of Atomic Energy, P. O. Box 275(10), Beijing 102413, China
(Received 15 January 2014; revised manuscript received 20 March 2014; published 28 April 2014)

Angular distributions of the ^{208}Pb(^{7}Li,^{6}He)^{209}Bi reactions with one-proton transferred to the ground, first-excited, and second-excited states of ^{209}Bi were measured at $E_{\rm lab} = 25.67$, 28.55, 32.55, 37.55, and 42.55 MeV. The experimental data and the data available in the literature at $E_{\rm lab} = 52$ MeV were analyzed within the theoretical framework of the distorted wave Born approximation and coupled reaction channels, respectively. The optical model potentials for the exotic system ^{6}He + ^{209}Bi, which is the exit channel of the reaction studied, have been extracted by means of fitting the angular distributions of transfer reactions. In the analyses, interaction potentials of the entrance channel ^{7}Li + ^{208}Pb were derived from the elastic scattering data. For the ^{6}He + ^{209}Bi system, the phenomenon of the so-called breakup threshold anomaly was observed. Furthermore, the angular distributions of elastic scattering and total reaction cross sections by direct measurement for the ^{6}He + ^{209}Bi system in the energy region near and above the Coulomb barrier can be satisfactorily reproduced by employing the potentials extracted through the transfer reactions.

DOI: 10.1103/PhysRevC.89.044615 PACS number(s): 24.10.Eq, 24.10.Ht, 25.70.Hi, 25.70.Bc

I. INTRODUCTION

The nuclear interaction is a fundamental ingredient in the study of mechanisms of nuclear reactions. The optical model potential (OMP) is universally adopted to phenomenologically describe the interaction of nuclear collisions. It is well known that the OMPs are closely related to the internal structures of the colliding nuclei, and the mechanisms of the nucleus-nucleus interaction at low energies is rather complicated due to coupling to internal degrees of freedom. Owing to the unusual structures of exotic nuclei, there has been a great deal of interest in reactions with weakly bound nuclei and halo nuclei over the past decades [1–8]. The availability of relatively intense beams of some radioactive nuclei has provided the opportunity to study the relevant elastic scattering and reactions induced by exotic nuclei. By employing new-generation detector arrays with large solid-angle coverage and high efficiency, elastic scattering and direct-reaction measurements with radioactive beams at multiple incident energies can now be made to almost the same degree of precision achieved with stable beams [9], e.g., in Refs. [10–15] rather accurate data have been reported. Among the exotic nuclei, ^{6}He has attracted enormous interest both theoretically and experimentally, due to its halo character [16,17], Borromean nature [18], as well as its large probability of breakup and/or transfer near the Coulomb barrier [19–21]. The recent results [10,11,22–28] obtained with a ^{6}He beam have clearly shown dramatic changes from the expected elastic scattering due to its exotic structure.

In spite of this impressive progress made in investigations related to exotic nuclei, we are still far from a clear understanding of the reaction mechanisms induced by exotic nuclei. This arises mainly from the experimental difficulties due to the limits of intensity and the quality of available radioactive ion beams (RIBs). Consequently, to date, the reaction systems as well as the reaction energies studied with RIBs are still limited. In view of this fact, if direct nucleus-nucleus scattering is impossible for some reason (e.g., unstable, short lived, and nonexisting in nature or for other reasons), the simplest transfer reactions can be used as an alternative method to study the interaction of exotic-nucleus systems in the exit channels [29–33]. In the present work, such an approach is applied for the ^{6}He + ^{209}Bi interaction by using the one-proton transfer reaction ^{208}Pb(^{7}Li,^{6}He)^{209}Bi. For this purpose, the angular distributions of the ^{7}Li + ^{208}Pb elastic scattering, as well as the ^{208}Pb(^{7}Li,^{6}He)^{209}Bi transfer reactions to the ground, the first-excited, and the second-excited states of ^{209}Bi were measured at energies near and above the Coulomb barrier. Together with the data set available in the literature [34], all the data sets were analyzed within the theoretical frameworks of the distorted wave Born approximation (DWBA) and coupled reaction channels (CRC). The single-particle strengths for both the ^{7}Li $\rightarrow$ ^{6}He + p and ^{209}Bi $\rightarrow$ ^{208}Pb + p systems have been determined through numerous experiments and theoretical calculations [35–39], so that the interactions in the incoming and outgoing channels can be studied in detail with the current new data. The phenomenological OMPs for the ^{7}Li + ^{208}Pb interaction were extracted from the elastic scattering of this system, which then establishes the incident-channel interaction, leaving that of the ^{6}He + ^{209}Bi as the only unknown interaction to be explored. Therefore, we could extract the phenomenological OMPs from the measured transfer angular distributions of the ^{208}Pb(^{7}Li,^{6}He)^{209}Bi reactions and study the energy dependence of the effective potentials for this exotic-nuclei system.

This paper is organized as follows: Section II contains a brief description of the experimental procedure. Section III gives the results of DWBA and CRC calculations for describing the data and makes detailed discussions on the OMPs extracted. A summary is presented in Sec. IV.

II. EXPERIMENTAL PROCEDURE

The experiment was carried out on the Q3D magnetic spectrometer at the China Institute of Atomic Energy, Beijing. A ^{208}Pb target with thickness of about 120 μg/cm^2 on a

*cjlin@ciae.ac.cn

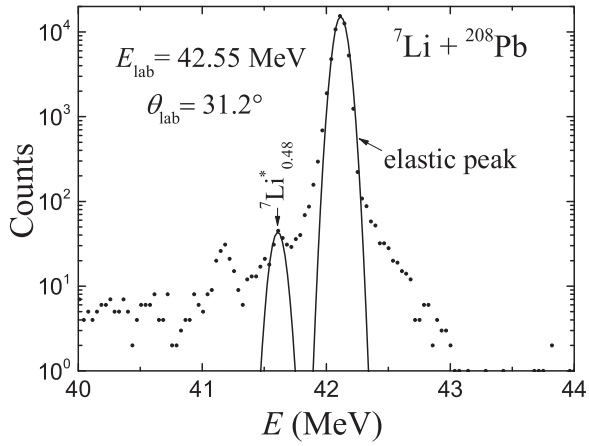

FIG. 1. Typical energy spectrum measured by the single Si(Au) detector at $E_{lab} = 42.55$ MeV and $\theta_{lab} = 31.2°$. Solid curves present the results of Gaussian fitting.

20 μg/cm^2 ^{12}C backing was bombarded by a ^{7}Li beam provided by the HI-13 tandem accelerator. Reaction energies in the laboratory system were 25.67, 28.55, 32.55, 37.55, and 42.55 MeV. The beam current on the target varied in the range of 5 to 20 pnA according to the measurement conditions. Two Si(Au) detectors were placed at $\pm 10°$ to monitor the current quality. In addition, a Faraday cup was used for the absolute measurement of the beam current. A detector array including seven Si(Au) surface-barrier detectors, with an interval of 10°, was mounted on a rotatable arm in the reaction chamber to detect scattering particles. The typical energy spectrum obtained by a single Si(Au) detector is shown in Fig. 1. The good energy resolution of the Si(Au) detectors allows us to separate the inelastic-scattering peak of the first-excited state of ^{7}Li ($E^* = 0.48$ MeV) from the elastic-scattering peak. Energy spectra were fitted by the sum of Gaussian functions with the peak positions fixed to the corresponding kinetic energies, as shown by the solid curves in Fig. 1. Finally, the elastic scattering angular distributions of ^{7}Li + ^{208}Pb at all the measured energies are shown in Fig. 2. Errors include statistical errors and fitting uncertainties.

Meanwhile, the Q3D magnetic spectrometer coupled with a multilayer position-sensitive focal plane gas detector was employed to select and detect the exited transfer products. P10 (90% Ar + 10% CH_4) gas was used as the working gas at a pressure of 400 mbar. The ΔE-E_R and ΔE-POS (position) spectra of the products recorded by the focal plane detector are shown in Figs. 3(a) and 3(b), respectively. The Q3D spectrometer with a high-moment resolution of $\Delta p/p \approx 10^{-4}$ can clearly separate the different ^{6}He groups yielded from

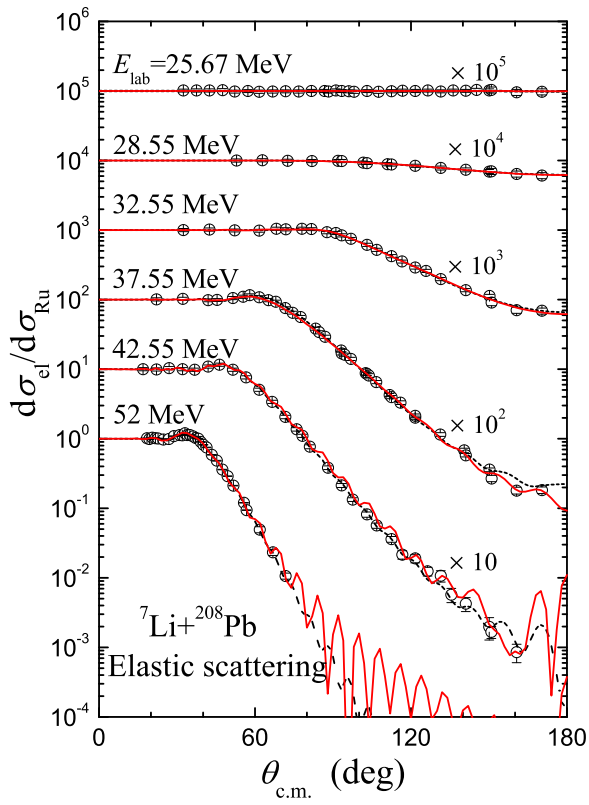

FIG. 2. (Color online) Angular distributions of elastic scattering of the ^{7}Li + ^{208}Pb system. Open circles represent the experimental data. Solid and dashed curves show the fitting results by the CRC and optical model (OM) calculations, respectively. The dataset of $E_{lab} = 52$ MeV was taken from Ref. [34].

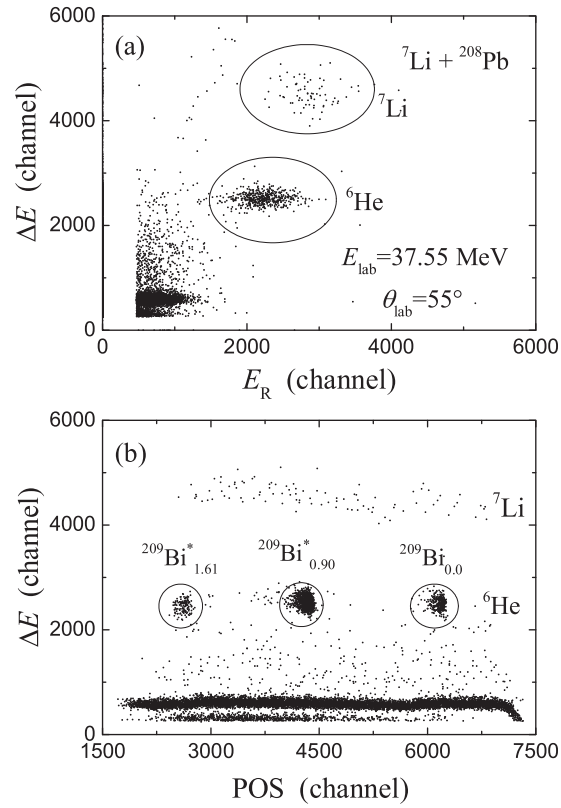

FIG. 3. (a) Typical ΔE-E_R spectrum and (b) ΔE-POS spectrum recorded by the focal plane detector at $E_{lab} = 37.55$ MeV and $\theta_{lab} = 55°$. The three groups of ^{6}He selected by circles correspond to one-proton transfers to the ground, the first-excited, and the second-excited states of ^{209}Bi, respectively.

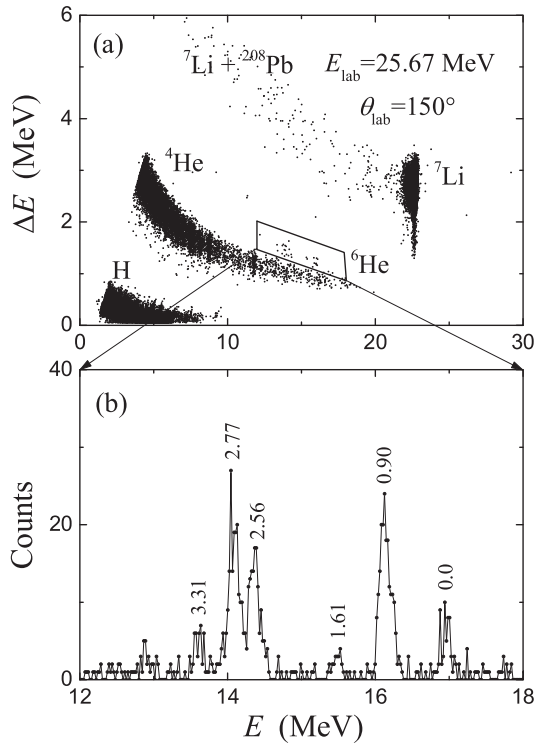

FIG. 4. (a) Typical ΔE-E spectrum obtained by the telescopes at $E_{lab} = 25.67$ MeV and $\theta_{lab} = 150^{\circ}$, and (b) the projected energy spectrum of the selected ^{6}He band, where numbers represent the excitation energy of ^{209}Bi, in units of MeV.

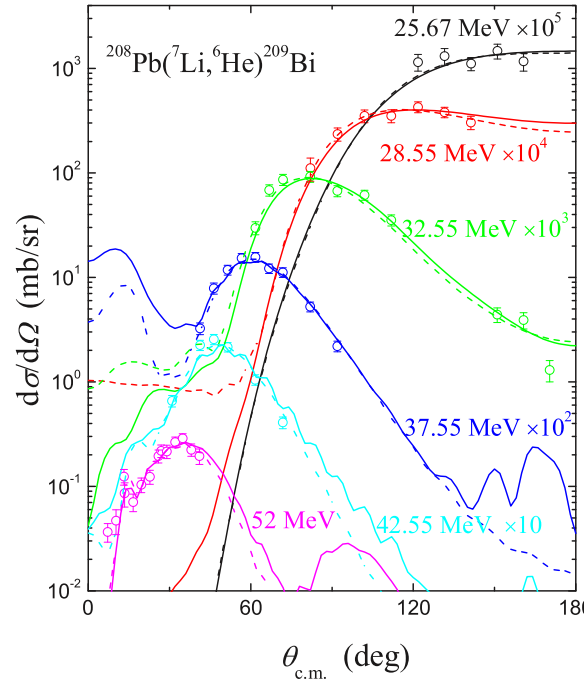

FIG. 5. (Color online) Angular distributions of ^{208}Pb(^{7}Li,^{6}He) reactions for transferring to the ground state of ^{209}Bi. The solid and dashed curves are the results of fitting by the CRC and DWBA methods, respectively. The dataset of $E_{lab} = 52$ MeV was taken from Ref. [34].

^{208}Pb(^{7}Li,^{6}He)^{209}Bi reactions, corresponding to stripping one proton from ^{7}Li to the ground, the first-excited state ($E^{*} = 0.90$ MeV) and the second-excited state ($E^{*} = 1.61$ MeV) of ^{209}Bi, as shown in Fig. 3(b). The angle range covered by the Q3D spectrometer is from -20° to 140°. In order to detect the transfer products in the range of backward angles, three ΔE-E Si(Au) telescopes were fixed at the backward angles of $\theta_{lab} = 150^{\circ}$, 160°, and 170° in the reaction chamber. Figure 4 shows the typical energy spectrum obtained by the telescope at $\theta_{lab} = 150^{\circ}$. One can find that more groups of ^{6}He yielded from the transfer reactions were observed, and they can be distinguished clearly. Finally, the transfer angular distributions of the ^{208}Pb(^{7}Li,^{6}He)^{209}Bi reactions to the ground, the first-excited, and the second-excited states of ^{209}Bi were obtained and are shown in Figs. 5–7, respectively. Only the statistic errors are considered for the transfer-reaction cross sections.

III. DATA ANALYSIS

A. OMP, DWBA, and CRC calculations

The OMP $V(r)$ is composed of the Coulomb potential $V_C(r)$ and nuclear potential $V_N(r)$,

$$V(r) = V_C(r) + V_N(r), \tag{1}$$

where

$$V_C(r) = \begin{cases} \frac{\left(3R_C^2 - r^2\right) Z_P Z_T e^2}{2R_C^2}, & r < R_C \\ \frac{Z_P Z_T e^2}{r}, & r \geqslant R_C, \end{cases} \tag{2}$$

with $R_C = r_{0C}(A_p^{1/3} + A_t^{1/3})$. Large variations in the Coulomb radius can be compensated by minor variations in the real potential [40] without appreciable change in the quality of the fit. Thus, the reduced Coulomb radius r_{0C} was kept constant at 1.30 fm throughout the analyses. The potential $V_N(r)$ is defined as

$$V_N(r) = V f_V(r) + i W f_W(r), \tag{3}$$

where V and W are the depths of the real and imaginary parts of the potential with Woods–Saxon form,

$$f_x(r) = \left\{1 + \exp\left[\frac{r - r_{0x}\left(A_P^{1/3} + A_T^{1/3}\right)}{a_x}\right]\right\}^{-1}, \quad x = V, W, \tag{4}$$

where Z_P, Z_T, and A_P, A_T are the charges and masses of the projectile and the target, respectively.

The DWBA method, as an extension of OM, is no doubt the most useful approximation in direct nuclear reaction theory. When the coupling to the intermediate channel is weak, it is reasonable to evaluate the transition amplitude with DWBA, which uses the distorted waves to represent the relative motion in the entrance and exit channels. However, when the coupling effects cannot be neglected, the

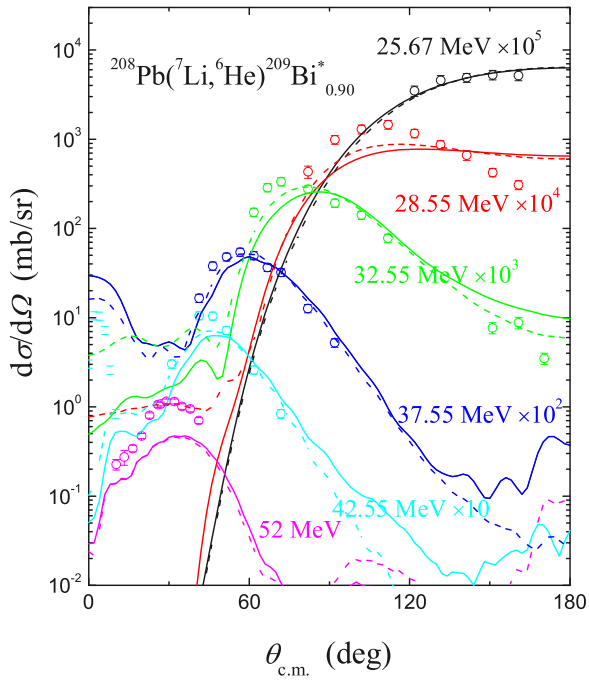

FIG. 6. (Color online) Same as Fig. 5, but for transferring to the first-excited state of ^{209}Bi.

coupled-channels technique is then adopted to include the couplings to the nuclear rearrangements, transfer reactions, or multiple-step processes. In the present work, the CRC method was used to take into account the coupling effects to the entrance and exit channels. In the CRC analysis, ^{7}Li + ^{208}Pb elastic and inelastic scattering for the transitions to the first-three excited states of ^{7}Li, as well as the reorientations of these states were included, as shown in Fig. 8(a). Excitations of ^{7}Li were described within a collective model other than the cluster model, in terms of deformed potentials. The strengths of the coupling factors for Coulomb and nuclear deformation can be described by

$$M(E\lambda) = \pm\sqrt{(2I+1)B(E\lambda; I \to I')} \tag{5}$$

and

$$RDEF(\lambda; I \to I') = (-1)^{(I-I'+|I-I'|)/2}\sqrt{(2I+1)} < IK\lambda_0 \mid I'K > \beta_\lambda R_0, \tag{6}$$

respectively, where I and I' are the angular momentum of the initial and the final states, λ is the transition multipolarity, $B(E\lambda; I \to I')$ is the transition probability, K is the projection of the angular momentum I and I' within a rotational model, β_λ is the deformation parameters, and R_0 is the radius of the sphere with the same volume. Moreover, one-proton and one-neutron transfer reactions from ^{7}Li to ^{208}Pb were also included in the coupled-channels scheme, and the diagrams are presented in Fig. 8(b).

In the calculation procedure, the bound-state wave functions were calculated by adjusting the potential depth V to reproduce the binding energy, with radius $R = r_0 A^{1/3}$ and diffuseness $a = 0.65$ fm. Instead of the nominally standard value $r_0 = 1.25$ fm, we chose the value $r_0 = 1.87$ fm and $r_0 = 1.21$ fm for ^{7}Li and ^{209}Bi, respectively, for reproducing the root-mean-square radii of ^{7}Li and ^{209}Bi, extracted from the $(e,e'p)$ reactions [38,39].

All the calculations in the present work were performed by the code FRESCO [41].

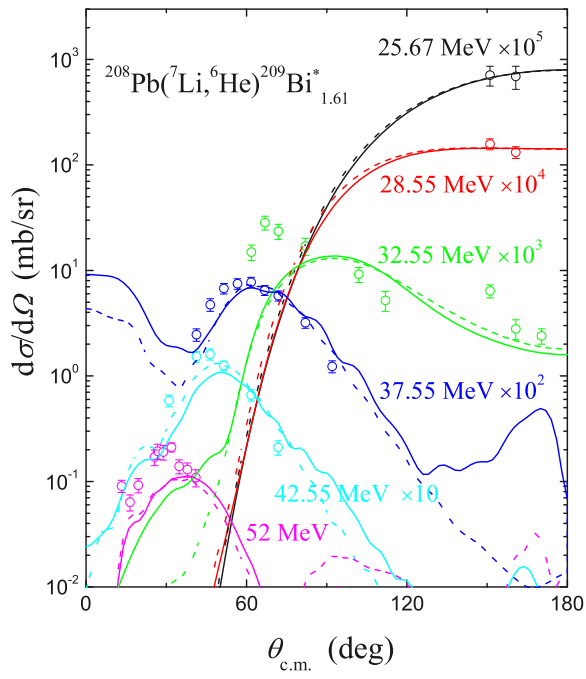

FIG. 7. (Color online) Same as Fig. 5, but for transferring to the second-excited state of ^{209}Bi.

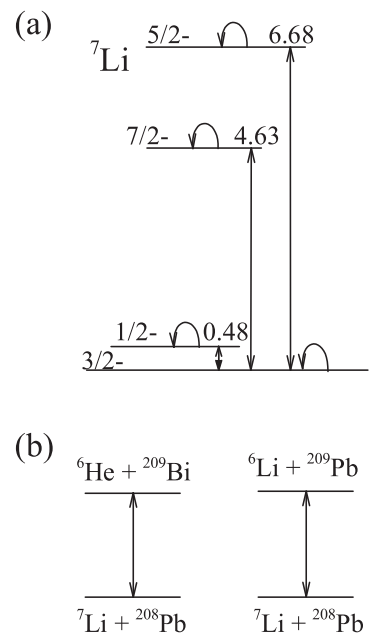

FIG. 8. Diagrams of the couplings of (a) the ground state of ^{7}Li to the excited states as well as their respective reorientations, and (b) elastic channels to transfer channels.

B. Elastic scattering of ^{7}Li + ^{208}Pb

To extract the reliable OMP of the ^{7}Li + ^{208}Pb system, the scattering data were fitted with the OM first. In the fitting procedure, a grid search on all the six potential parameters $\{X_i\} = \{V, r_{0V}, a_V, W, r_{0W}, a_W\}$ was carried out to obtain the best fit to the angular distributions at different bombarding energies. For each angular distribution of N data points, the "goodness of fit" quantity χ^2 was calculated as

$$\chi^2 = \sum_{i=1}^{N} \left[\frac{\sigma_{\rm th}(\theta_i) - \sigma_{\rm exp}(\theta_i)}{\Delta\sigma_{\rm exp}(\theta_i)} \right]^2, \qquad (7)$$

where $\sigma_{\rm th}(\theta_i)$, $\sigma_{\rm exp}(\theta_i)$, and $\Delta\sigma_{\rm exp}(\theta_i)$ are the calculated cross section, the experimental cross section, and its associated error at each angle θ_i, respectively. The best-fitting results are shown in Fig. 2 as the dashed lines.

Then, the obtained OMP parameters were used as the initial values in the CRC fit. The fitting results are shown in Fig. 2 by the solid curves. Finally, the OMP parameters of ^{7}Li + ^{208}Pb extracted by the OM and CRC calculations, as well as the χ^2 per point (χ^2/pt) are listed in Table I. Besides our experimental data, the dataset taken from the literature [34] at $E_{\rm lab} = 52$ MeV was also analyzed with the same procedure.

As shown in Fig. 2, one can find that, for the forward angles, the descriptions of the angular distributions by OM and CRC calculations are indistinguishable. Nevertheless, for the backward-angle area, where the inelastic scattering and multistep processes become important, the CRC calculations can optimize the fitting results further. On the other hand, as listed in Table I, one can find that there still exists an energy dependence for the OMPs derived from the CRC method, indicating that it is not a "bare" potential. Similar results were obtained in Ref. [42], where the scattering of polarized ^{7}Li from a ^{208}Pb target was analyzed. It might result from the $\alpha + t$ cluster structure of ^{7}Li, for which the collective model could not describe it well.

TABLE I. The OMP parameters of ^{7}Li + ^{208}Pb extracted from elastic scattering by the OM and CRC calculations.

	$E_{\rm lab}$ MeV	V MeV	r_{0V} fm	a_V fm	W MeV	r_{0W} fm	a_W fm	χ^2/pt
OM	25.67	8.02	1.33	0.58	3.45×10^{-4}	1.22	0.52	0.12
	28.55	13.33	1.10	0.62	2.38	1.50	0.68	0.63
	32.55	16.10	1.26	0.56	2.58	1.48	0.51	0.33
	37.55	37.11	1.26	0.56	2.19	1.48	0.51	1.43
	42.55	61.23	1.23	0.54	5.23	1.30	0.78	0.27
	52[a]	103.20	1.11	0.67	7.11	1.29	0.83	5.25
CRC	25.67	4.05	1.37	0.56	8.52×10^{-5}	1.24	0.53	0.11
	28.55	10.32	1.30	0.53	1.30	1.48	0.91	0.68
	32.55	15.84	1.34	0.50	1.92	1.49	0.49	0.36
	37.55	35.81	1.27	0.54	1.88	1.52	0.41	1.32
	42.55	64.28	1.23	0.54	3.47	1.30	0.78	0.22
	52[a]	109.76	1.07	0.77	6.67	1.33	0.44	5.18

[a]The experimental data is taken from Ref. [34].

C. Analysis of ^{208}Pb(^{7}Li,^{6}He)^{209}Bi data

The angular distributions of the one-proton transfer reactions ^{208}Pb(^{7}Li,^{6}He)^{209}Bi were fitted with the DWBA and CRC methods, respectively, to extract the OMPs of the halo system ^{6}He + ^{209}Bi as the exit channel. The energy dependence of the OMPs extracted was analyzed. Furthermore, the elastic scattering, as well as the total cross sections of the ^{6}He + ^{209}Bi system were calculated with the OMPs we deduced and compared with the experimental data to inspect the feasibility of the transfer method. Details are described in the following:

1. *OMPs of ^{6}He + ^{209}Bi system*

The transfer-reaction data of ^{208}Pb(^{7}Li,^{6}He)^{209}Bi, as well as the data taken from Ref. [34] at $E_{\rm lab} = 52$ MeV, were first analyzed by the DWBA method. After a grid search of the all six OMP parameters for the exit channel of the ^{6}He + ^{209}Bi system, the average geometry parameters were extracted as $r_{0V} = 1.02$ fm, $a_V = 0.70$ fm, $r_{0W} = 1.25$ fm, and $a_W = 0.95$ fm, which are compatible with the ones taken from Refs. [13,28,43]. One can find that the radius and diffuseness parameters of the imaginary potential are obviously larger than those of the real part. This indicates that the absorption of flux from the elastic channel of ^{6}He + ^{209}Bi starts to occur at long distances, as should be expected for projectiles with halo structure, for which it has already been shown that polarization potentials have a long tail due to the presence of the breakup channel [43–45]. Furthermore, in order to reduce the ambiguity of the fitting results, the potential depths V and W were searched again by the DWBA and CRC methods, respectively, with r_{0i} and a_i ($i = V, W$) fixed at the average values. The OMP parameters obtained by the DWBA and CRC methods and the reaction cross sections $\sigma_{\rm R}$ calculated by the corresponding OMPs for the ^{6}He + ^{209}Bi system are listed in Table II.

The reaction energy of the ^{6}He + ^{209}Bi system as the exit channel can be calculated as

$$E_{\rm c.m.}(^{6}{\rm He}) = E_{\rm c.m.}(^{7}{\rm Li}) + Q - E^*(^{209}{\rm Bi}), \qquad (8)$$

where $E_{\rm c.m.}(^{7}$Li) is the center-of-mass energy of the entrance channel, Q is the Q value of the transfer reaction, and $E^*(^{209}$Bi) is the excitation energy of residue nuclei ^{209}Bi.

In principle, in the DWBA or CRC calculations, all the excited states of ^{209}Bi could be contained to fit all the distributions simultaneously. However, as shown in Eq. (8), different states of ^{209}Bi correspond to different reaction energies of the ^{6}He + ^{209}Bi system. Therefore, corresponding to each bombarding energy, only the average OMPs could be extracted through simultaneous fitting. According to the experiences of the tightly bound systems, the OMPs varied drastically with energy around the Coulomb barrier, where the average OMPs could not represent correctly the variation trend. In view of this, only one state of ^{209}Bi was included each time, and the corresponding distribution was fitted. Thus, the OMPs of ^{6}He + ^{209}Bi with ^{209}Bi populated in different states could be extracted, which allowed us to discuss the variation tendency of the OMPs more finely.

The fitting results are shown in Figs. 5–7 by the dashed and solid curves, respectively. Overall, the experimental angular distributions can be reproduced satisfactorily by both the

TABLE II. OMP strengths of real (V) and imaginary (W) parts, χ^2/pt values and reaction cross sections for the ^{6}He + ^{209}Bi system, by the analysis of DWBA and CRC methods. The OMP geometry parameters were fixed as $r_{0V} = 1.02$ fm, $a_V = 0.70$ fm, $r_{0W} = 1.25$ fm, and $a_W = 0.95$ fm.

$E_{lab}(^7Li)$	$E^*(^{209}Bi)$[a]	$E_{lab}(^6He)$[b]	DWBA				CRC			
MeV	MeV	MeV	V MeV	W MeV	χ^2/pt	σ_R mb	V MeV	W MeV	χ^2/pt	σ_R mb
25.67	0.00	19.19	799.95	16.67	0.96	496.03	579.99	24.39	1.13	563.27
	0.90	18.27	400.05	20.05	0.88	308.56	290.01	32.05	0.67	420.39
	1.61	17.54	32.00	62.05	0.11	456.23	22.05	52.05	0.12	401.89
28.55	0.00	22.06	600.05	7.76	0.27	887.64	500.05	13.20	0.64	986.43
	0.90	21.13	730.00	9.05	10.94	775.82	600.07	22.40	15.51	970.46
	1.61	20.40	1000.05	35.50	0.47	1014.58	805.15	25.50	0.49	884.01
32.55	0.00	26.04	400.00	7.86	2.87	1426.89	322.95	12.50	2.83	1530.09
	0.90	25.11	310.00	5.87	6.88	1187.03	200.05	12.05	13.57	1336.25
	1.61	24.38	449.95	25.05	13.05	1581.05	350.05	15.05	13.54	1365.64
37.55	0.00	31.01	309.95	11.64	0.71	2039.25	266.62	16.49	0.70	2162.73
	0.90	30.09	248.33	6.00	3.05	1705.94	166.14	13.05	7.48	1932.08
	1.61	29.36	212.98	5.00	5.18	1558.91	148.79	8.60	5.25	1683.86
42.55	0.00	35.99	219.78	10.35	1.63	2359.55	219.78	18.60	2.71	2590.00
	0.90	35.07	291.18	7.27	6.95	2176.34	157.52	13.05	14.29	2332.89
	1.61	34.33	190.11	5.46	5.35	1963.36	175.52	13.50	12.10	2308.45
52 [c]	0.00	45.39	197.80	11.05	2.62	2792.80	195.00	20.10	2.59	3101.07
	0.90	44.47	230.00	11.50	52.48	2795.46	200.05	16.50	49.63	2961.17
	1.61	43.74	219.95	11.50	28.38	2761.07	165.05	19.50	23.48	3009.65

[a]The excitation energy of ^{209}Bi as the final state of ^{208}Pb(^{7}Li,^{6}He)^{209}Bi.
[b]The corresponding reaction energy of the ^{6}He + ^{209}Bi system.
[c]The experimental dataset is taken from Ref. [34].

DWBA and CRC calculations. But the agreements for excited states are not good as the one for the ground state. It might result from the improper use of the bound-state interaction radius r_V for the excited states of ^{209}Bi. In the calculations, the ground-state value was adopted for the excited states because there is no experimental information on these values.

Meanwhile, the average spectroscopic factors for the ground and the first-two excited states of ^{209}Bi were extracted by comparison between the calculations and experimental data and with the spectroscopic factors of ^{7}Li kept fixed at 0.60 [46]. The spectroscopic factors obtained are shown and compared with those of Refs. [37,47,48] in Table III. The errors come from the uncertainties of the fitting procedure. In Ref. [47], the spectroscopic factors are obtained from the theoretical calculations. The values from Ref. [48] are extracted from the reaction ^{208}Pb(^{3}He,d)^{209}Bi. And in Ref. [37], the spectroscopic factors are deduced from the ^{208}Pb(α,t)^{209}Bi reaction. One can note that there are certain variations in the reported spectroscopic factors derived from various reactions. The results of this work are comparable to those given in Ref. [48].

2. *Breakup threshold anomaly of ^{6}He + ^{209}Bi*

It is well known that, for the elastic scattering between heavy ions at energies close to the Coulomb barrier, the real and imaginary parts of the OMP show an energy dependence, known as the threshold anomaly (TA) [49–51]. This behavior is characterized by the rapid decrease of the imaginary part of the potential as the bombarding energy decreases from above barrier towards below barrier, while the real part of the potential presents a localized peak around the barrier. The real part of the energy-dependent potential $V(r;E)$ can be expressed as

$$V(r;E) = V_0(r;E) + \Delta V(r;E), \tag{9}$$

where $V_0(r;E)$ is slowly and smoothly energy dependent, which arises from the nonlocality effects, and $\Delta V(r;E)$ is the dynamic polarization potential, which is a consequence

TABLE III. Deduced spectroscopic factors for ^{209}Bi.

State	E^* (MeV)	DWBA[a]	CRC[b]	Ref. [47]	Ref. [48]	Ref. [37]
$1h_{9/2}$	0.00	1.07 ± 0.05	1.16 ± 0.04	0.95	1.17	0.80
$2f_{7/2}$	0.90	0.88 ± 0.04	0.87 ± 0.05	0.85	0.78	0.76
$1i_{13/2}$	1.61	0.43 ± 0.11	0.49 ± 0.11	0.70	0.56	0.74

[a]Results of this work with the analysis of the DWBA method.
[b]Results of this work with the analysis of the CRC method.

of the causality principle and links to the imaginary potential $W(r; E)$ through the dispersion relation

$$\Delta V(r; E) = \frac{\mathrm{P}}{\pi} \int \frac{W(r; E')}{E' - E} dE', \tag{10}$$

where P denotes the principal value of the integral. Although this effect is well established for the scattering of tightly bound nuclei, for systems involving weakly bound nuclei, such as ^{6}Li, ^{7}Li, and ^{9}Be, this situation may change substantially [52–58]. In those systems, couplings to breakup channels continue to be important even for energies below the barrier, thus the imaginary potentials could even increase at lower energies. This is the so-called breakup threshold anomaly (BTA).

So far, the BTA phenomenon has been observed only for a few systems including halo or neutron skin nuclei [43,59]. Actually, it is a very difficult task for such systems to measure the elastic scattering directly due to the low intensities of secondary beams, which will result in large statistical errors. However, via the transfer reactions, we have the opportunity to study the energy-dependent potentials of the exotic system, ^{6}He + ^{209}Bi, with higher precision in a wider energy range. In order to investigate the BTA phenomenon of the ^{6}He + ^{209}Bi system, the sensitivity radius R_s was extracted first by varying the diffuseness parameters a_V and a_W, respectively, in steps of 0.02 fm, while the depth values were fitted again [60]. The average sensitivity radius was derived as $R_s = 13.50$ fm, for both real and imaginary parts of the potential. Figure 9 shows that the depths of the real and imaginary potentials extracted by the CRC (solid circles) and DWBA (open squares) methods, respectively, varying with the center-of-mass energy. The errors of potential depths were derived by χ^2 analysis, i.e., determined by $\chi^2_{\min} + 1$ for the procedure when the single parameter was fitted, corresponding to a confidence level of 68.3%. One can find that the errors become large for the sub-barrier-energy range. This manifests that the interaction below the Coulomb barrier may become insensitive to the depths of the OMP. As shown in Fig. 9(b), in the sub-barrier-energy region, one can find that both the CRC and DWBA fitting results present a clear increasing trend of the imaginary potential strength, the same BTA phenomena as the ones observed in stable weakly bound systems. In the energy region above the Coulomb barrier, however, the depths of the imaginary potential varied around an average value. And compared to the imaginary potential strengths extracted by the DWBA method, the ones obtained by the CRC method were slightly deeper.

According to the dispersion relation, if W decreases with increasing energy in a narrow range, the corresponding ΔV will generate a strong repulsive effect in the same energy range [50]. However, in contrast to this, a sharp peak appears in the real part of the OMP, which manifests itself as an attractive potential, as shown in Fig. 9(a). In fact, the suggestion that the dispersion relation is of no use in the weakly bound system has already been offered in Refs. [50,61]. Although in Refs. [43,54,59] the authors tried to use the dispersion relation to describe the connection of the real and imaginary parts of the OMP of weakly bound systems, due to the large errors and few data points, it is hard to draw a specific conclusion. Therefore, whether the dispersion relation is suitable for the weakly bound system is still an open question that deserves further investigation.

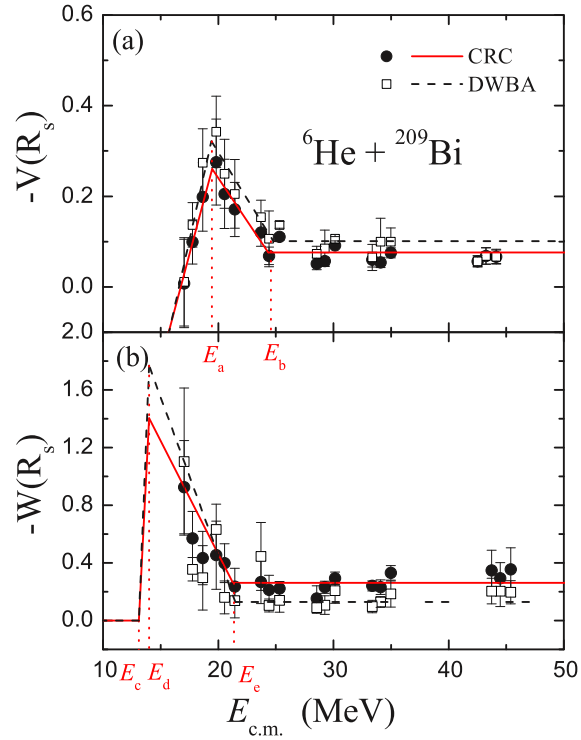

FIG. 9. (Color online) Energy dependence of (a) real and (b) imaginary parts of the OMP at the sensitivity radius of 13.5 fm. The full circles and empty squares represent the results extracted by the CRC and DWBA methods, respectively. The solid and dashed curves show the linear segment fitting results for the real and imaginary potentials.

Moreover, the strengths of the real part obtained by both the CRC and DWBA methods manifest a strong polarization effect in the lower-energy region, as shown in Fig. 9(a). This feature is consistent with the long-range Coulomb dipole polarization (CDP) potential, whose simple analytical expression has been derived in Refs. [62,63], leading to the large enhancement of the α-emission cross section of ^{6}He + ^{209}Bi scattering [27,28]. This large yield of α particles was due to the electric dipole ($E1$) excitation of ^{6}He to its continuum states; that is, the Coulomb breakup process of ^{6}He. However, for this system, experiments [64,65] show that one- and two-neutron transfer channels have large cross sections near the Coulomb barrier, and approximately 75% of the observed α-particle yield is because of these two processes. Therefore, it still needs to be investigated further whether these transfer channels or the Coulomb breakup process of ^{6}He in the sub-barrier energy region are responsible for the apparent BTA observed.

3. *Reproduction of elastic scattering data and reaction cross sections for ^{6}He + ^{209}Bi system*

There exists one set of experimental data for the ^{6}He + ^{209}Bi system, reported in Refs. [27,28] for $E_{\mathrm{c.m.}}(^6\mathrm{He}) = 14.3$, 15.8, 17.3, 18.6, and 21.4 MeV. In order to compare the calculated results with the OMP parameters obtained in the

present work, with the existing experimental dataset, the analyses of the energy dependence of the derived parameters were performed. Due to the inapplicability of the dispersion relation, the simplest linear-segment representations were adopted to describe the systematics of energy-dependent potentials:

$$V(E_{\mathrm{c.m.}}) = \begin{cases} 0.095E_{\mathrm{c.m.}} - 1.60, & E_{\mathrm{c.m.}} \leqslant E_a \\ -0.039E_{\mathrm{c.m.}} + 1.02, & E_a \leqslant E_{\mathrm{c.m.}} \leqslant E_b \\ 0.076, & E_{\mathrm{c.m.}} \geqslant E_b, \end{cases} \tag{11}$$

$$W(E_{\mathrm{c.m.}}) = \begin{cases} 0, & E_{\mathrm{c.m.}} \leqslant E_c \\ 0.33E_{\mathrm{c.m.}} - 4.28, & E_c \leqslant E_{\mathrm{c.m.}} \leqslant E_d \\ -0.16E_{\mathrm{c.m.}} + 3.60, & E_d \leqslant E_{\mathrm{c.m.}} \leqslant E_e \\ 0.26, & E_{\mathrm{c.m.}} \geqslant E_e, \end{cases} \tag{12}$$

and

$$V(E_{\mathrm{c.m.}}) = \begin{cases} 0.11E_{\mathrm{c.m.}} - 1.90, & E_{\mathrm{c.m.}} \leqslant E_a \\ -0.041E_{\mathrm{c.m.}} + 1.11, & E_a \leqslant E_{\mathrm{c.m.}} \leqslant E_b \\ 0.10, & E_{\mathrm{c.m.}} \geqslant E_b, \end{cases} \tag{13}$$

$$W(E_{\mathrm{c.m.}}) = \begin{cases} 0, & E_{\mathrm{c.m.}} \leqslant E_c \\ 0.24E_{\mathrm{c.m.}} - 3.11, & E_c \leqslant E_{\mathrm{c.m.}} \leqslant E_d \\ -0.22E_{\mathrm{c.m.}} + 4.85, & E_d \leqslant E_{\mathrm{c.m.}} \leqslant E_e \\ 0.13, & E_{\mathrm{c.m.}} \geqslant E_e, \end{cases} \tag{14}$$

for the CRC and DWBA results, respectively, where the energies are given in units of MeV, and $E_a = 19.44$ MeV, $E_b = 24.65$ MeV, $E_c = 13.12$ MeV, $E_d = 14.00$ MeV, $E_e = 21.37$ MeV, as labeled in Fig. 9. E_c is the energy where the imaginary potential began to vanish, as does the total cross section. Therefore, the value of E_c is determined by the excitation function of this system, which will be discussed later. E_d is the energy from which the strength of the imaginary part starts to drop to zero as the energy decreases. However, it cannot be determined accurately with the existing experimental data, and it was pointed out in Ref. [43] that the variation of the value of E_d only slightly modifies the shape of the real part. Therefore, the choice of the value of E_d is arbitrary.

The obtained OMP parameters for the exit channels is one kind of effective interaction potential, included all the coupling and related dynamical effects. Therefore, we could utilize these parameters directly in the simple OM calculations to get theoretical angular distributions of elastic scattering for the ^{6}He + ^{209}Bi system. Calculation results with the systematic energy-dependent OMP parameters discussed above are compared with the experimental data reported in Refs. [27,28], as shown in Fig. 10, where the solid and dashed curves represent the calculation results with the parameters obtained by the CRC and DWBA methods, respectively.

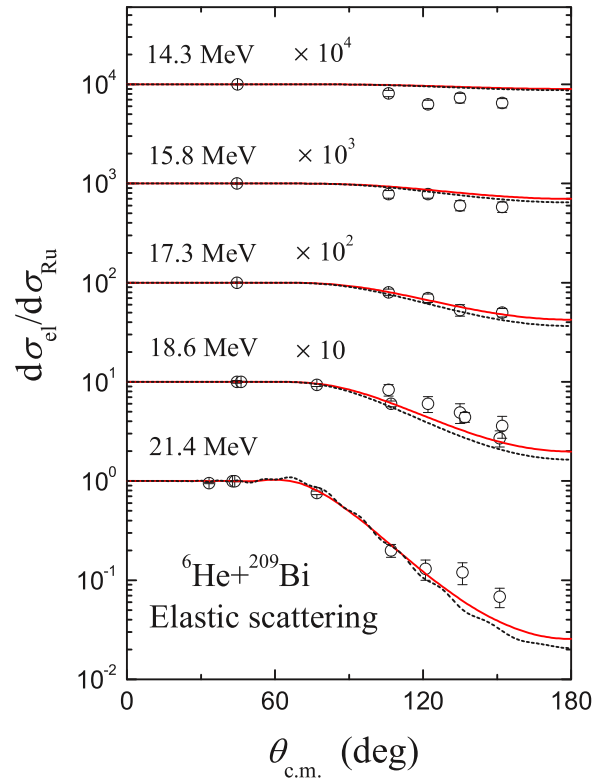

FIG. 10. (Color online) Elastic scattering angular distributions of the ^{6}He + ^{209}Bi system. Open circles are the experimental data taken from Refs. [27,28]. The solid and dashed curves are the calculation results with the systematic OMP parameters extracted through the CRC and DWBA methods, respectively.

At the lowest energy, calculation results with both the CRC and DWBA parameters overestimate the experimental data. The reason for that might be due to the uncertainty in the normalization of the experimental data owing to the intrinsic difficulty at such a low energy [43]. Except for the lowest energy point, the theoretical curves calculated with both DWBA and CRC parameters could describe the experimental angular distributions satisfactorily over the whole energy and angle range. Results with the CRC parameters seem slightly better than those with the DWBA parameters.

Moreover, the total reaction cross section σ_{R} is one of the most important observable that can be calculated by the optical model. In Fig. 11, σ_{R} values calculated by CRC and DWBA parameters at each energy are plotted as solid circles and open squares, respectively. Meanwhile, results with systematic energy-dependent OMPs derived from CRC and DWBA parameters are also shown as the solid and dashed curves, respectively. The experimental σ_{R} data taken from Refs. [27,28] are further presented by solid triangles for comparison. These experimental data are results of sums of fusion, transfer, and breakup yields. It can be seen that the calculated cross sections are in reasonable agreement with the experimental data, except in the extremely-low-energy region, where theoretical predictions underestimate the experimental reaction cross sections.

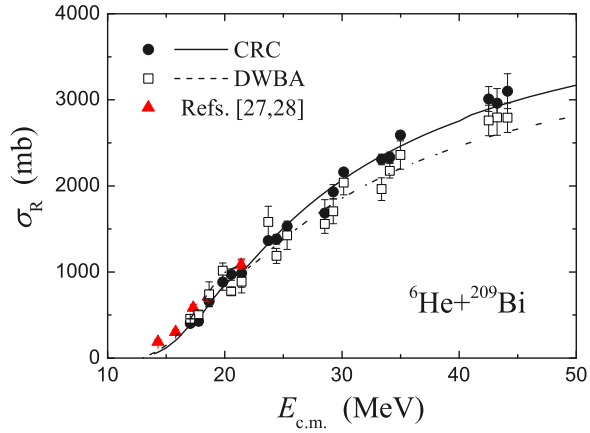

FIG. 11. (Color online) Excitation function of the total reaction cross section for the ^{6}He + ^{209}Bi system. Solid triangles are experimental results taken from Refs. [27,28], solid circles and open squares are the calculated results with the OMP parameters extracted by the CRC and DWBA methods, respectively, and solid and dashed cures are predicated values by the systematic energy-dependent OMPs described by Eqs. (11) to (14) obtained from the CRC and DWBA methods, respectively.

Through the comparison between the calculation results with the CRC and DWBA parameters, one can find that there still exists a little difference, although they are reasonably consistent with each other. The reason behind this diversity is that, in the DWBA calculations, the influence from the entrance channel, ^{7}Li + ^{208}Pb, could not be excluded. Nevertheless, this problem could be solved partly by the CRC method, which introduces an additional nonorthogonality correction in the coupled equations. In principle, if the effects of the full coupled channels were included in the CRC calculations in the transfer method, the pure effective interaction of the exotic system ^{6}He + ^{209}Bi could be extracted.

IV. SUMMARY AND CONCLUSIONS

In the present work, the angular distributions of the ^{208}Pb(^{7}Li,^{6}He)^{209}Bi transfer reactions with the residue nucleus ^{209}Bi populated in the ground, the first-excited, and the second-excited states as well as ^{7}Li + ^{208}Pb elastic scattering were measured at $E_{lab} = 25.67$, 28.55, 32.55, 37.55, and 42.55 MeV. The interaction OMPs for the ^{7}Li + ^{208}Pb system were extracted from the measured elastic scattering angular distributions in terms of the fitting procedure with OM and CRC calculations. We found that the CRC calculation could optimize the fitting results further for this weakly bound system in the backward-angle area, where inelastic scattering and multistep reactions are important.

By using the deduced OMP parameters of ^{7}Li + ^{208}Pb as the interaction of the entrance channel, the angular distributions of the ^{208}Pb(^{7}Li,^{6}He)^{209}Bi transfer reactions were analyzed by the DWBA and CRC methods, and the interaction OMP parameters of the exotic system ^{6}He + ^{209}Bi were extracted. The OMP parameters obtained by the two methods are almost the same. Moreover, the energy dependence of the OMP parameters were deduced. The results obviously display the so-called BTA phenomenon for the ^{6}He + ^{209}Bi system. However, the dispersion relation cannot predict the shape of the real part of the OMP, which should be investigated further. Furthermore, we calculated the angular distributions of elastic scattering, as well as the total reaction cross sections for the the ^{6}He + ^{209}Bi system within the OM and compared with the experimental results. The calculated results with the OMP parameters extracted through this transfer method with the CRC analysis are in agreement with the experimental data in the energy region near and above the Coulomb-barrier energy region. It can be concluded that the OMP parameters extracted with the transfer method for the ^{6}He + ^{209}Bi system is reliable. Therefore, when direct nucleus-nucleus scattering is difficult or impossible to measure, the transfer reaction as an alternative method could provide a useful and sensitive tool for extracting the OMP parameters of exotic reaction systems.

ACKNOWLEDGMENTS

This work was supported by the National Key Basic Research Program of China (Grant No. 2013CB834404) and the National Natural Science Foundation of China (Grants No. 10735100, No. 11005156, No. 11005154, No. 11075216, and No. 11375268).

[1] Yu. E. Penionzhkevich, Nucl. Phys. A **616**, 247c (1997).
[2] F. D. Becchetti, W. Z. Liu, K. Ashktorab *et al.*, Phys. Rev. C **48**, 308 (1993).
[3] K. Kalita, S. Verma, R. Singh *et al.*, Phys. Rev. C **73**, 024609 (2006).
[4] I. Pecina, R. Anne, D. Bazin *et al.*, Phys. Rev. C **52**, 191 (1995).
[5] W. von Oertzen, Z. Phys. A **310**, 275 (1983).
[6] E. Liénard, D. Baye, T. Delbar *et al.*, Phys. Rev. C **52**, 775 (1995).
[7] T. Motobayashi, Phys. Lett. B **264**, 259 (1991).
[8] D. R. Tilley, H. R. Weller, and C. M. Cheves, Nucl. Phys. A **564**, 1 (1993).
[9] N. Keeley, N. Alamanos, K. W. Kemper, and K. Rusek, Prog. Part. Nucl. Phys. **63**, 396 (2009).
[10] M. Milin, S. Cherubini, T. Davinson *et al.*, Nucl. Phys. A **730**, 285 (2004).
[11] E. A. Benjamim, A. Lepine-Szily, D. R. Mendes Junior *et al.*, Phys. Lett. B **647**, 30 (2007).
[12] O. R. Kakuee, M. A. G. Alvarez, M. V. Anders *et al.*, Nucl. Phys. A **765**, 294 (2006).
[13] Y. Kucuk, I. Boztosun, and T. Topel, Phys. Rev. C **80**, 054602 (2009).
[14] A. Di Pietro, V. Scuderi, A. M. Moro *et al.*, Phys. Rev. C **85**, 054607 (2012).
[15] M. Cubero, J. P. Fernandez-Garcia, M. Rodriguez-Gallardo *et al.*, Phys. Rev. Lett. **109**, 262701 (2012).
[16] I. Tanihata, H. Hamagaki, O. Hashimoto *et al.*, Phys. Rev. Lett. **55**, 2676 (1985).

[17] I. Tanihata, Phys. Lett. B **160**, 380 (1985).
[18] J. M. Bang, Phys. Rep. **264**, 27 (1996).
[19] A. M. Sanchez Benitez *et al.*, J. Phys. G **31**, S1953 (2005).
[20] R. J. Smith, J. J. Kolata, K. Lamkin *et al.*, Phys. Rev. C **43**, 761 (1991).
[21] J. S. Al-Khalili *et al.*, Phys. Lett. B **378**, 45 (1996).
[22] L. R. Gasques, L. C. Chamon, D. Pereira *et al.*, Phys. Rev. C **67**, 024602 (2003).
[23] A. Di Pietro, P. Figuera, F. Amorini *et al.*, Phys. Rev. C **69**, 044613 (2004).
[24] A. Chatterjee, A. Navin, A. Shrivastava *et al.*, Phys. Rev. Lett. **101**, 032701 (2008).
[25] O. R. Kakuee, J. Rahighi, A. M. Sanchez-Benitez *et al.*, Nucl. Phys. A **728**, 339 (2003).
[26] A. M. Sanchez-Benitez, D. Escrig, M. A. G. Alvarez *et al.*, Nucl. Phys. A **803**, 30 (2008).
[27] E. F. Aguilera, J. J. Kolata, F. M. Nunes *et al.*, Phys. Rev. Lett. **84**, 5058 (2000).
[28] E. F. Aguilera, J. J. Kolata, F. D. Becchetti *et al.*, Phys. Rev. C **63**, 061603(R) (2001).
[29] V. M. Kyryanchuk, A. T. Rudchik, A. Budzanowski *et al.*, Nucl. Phys. A **726**, 231 (2003).
[30] G. P. An *et al.*, Chin. Phys. Lett. **25**, 4237 (2008).
[31] Z. D. Wu *et al.*, Chin. Phys. Lett. **26**, 022503 (2009).
[32] C. J. Lin *et al.*, AIP Conf. Proc. **853**, 81 (2006).
[33] A. T. Rudchik, Yu. M. Stepanenko, K. W. Kemper *et al.*, Nucl. Phys. A **831**, 139 (2009).
[34] A. F. Zeller, D. C. Weisser, T. R. Ophel, and D. F. Hebbard, Nucl. Phys. A **332**, 515 (1979).
[35] S. Cohen and D. Kurath, Nucl. Phys. A **101**, 1 (1967).
[36] K. S. Low and T. Tamura, Phys. Rev. C **11**, 789 (1976).
[37] S. Gales, C. P. Massolo, S. Fortier, J. P. Schapira, P. Martin, and V. Comparat, Phys. Rev. C **31**, 94 (1985).
[38] L. Lapikas, J. Wesseling, and R. B. Wiringa, Phys. Rev. Lett. **82**, 4404 (1999).
[39] D. Branford, A. W. Rauf, J. Lac *et al.*, Phys. Rev. C **63**, 014310 (2000).
[40] G. Bassani *et al.*, Nucl. Phys. A **189**, 353 (1972).
[41] I. J. Thompson, Comp. Phys. Rep. **7**, 167 (1988).
[42] I. Martel, J. Gómez-Camacho, C. O. Blyth *et al.*, Nucl. Phys. A **582**, 357 (1995).
[43] A. R. Garcia, J. Lubian, I. Padron *et al.*, Phys. Rev. C **76**, 067603 (2007).
[44] J. Lubian and F. M. Nunes, J. Phys. G **34**, 513 (2007).
[45] T. Matsumoto, T. Egami, K. Ogata, Y. Iseri, M. Kamimura, and M. Yahiro, Phys. Rev. C **73**, 051602(R) (2006).
[46] A. M. Moro, J. Gómez-Camacho, I. Martel *et al.*, Nucl. Phys. A **628**, 203 (1998).
[47] P. Ring and E. Werner, Nucl. Phys. A **211**, 198 (1973).
[48] C. Ellegard and P. Vedelsby, Phys. Lett. B **26**, 155 (1968).
[49] M. A. Nagarajan, C. C. Mahaux, and G. R. Satchler, Phys. Rev. Lett. **54**, 1136 (1985).
[50] C. Mahaux, H. Ngô, and G. R. Satchler, Nucl. Phys. A **449**, 354 (1986).
[51] G. R. Satchler, Phys. Rep. **199**, 147 (1991).
[52] N. Keeley, S. J. Bennett, N. M. Clarke *et al.*, Nucl. Phys. A **571**, 326 (1994).
[53] C. Signorini *et al.*, Phys. Rev. C **61**, 061603(R) (2000).
[54] M. S. Hussein, P. R. S. Gomes, J. Lubian, and L. C. Chamon, Phys. Rev. C **73**, 044610 (2006).
[55] J. M. Figueira, D. Abriola, J. O. Fernandez Niello *et al.*, Phys. Rev. C **73**, 054603 (2006).
[56] J. O. Fernandez Niello, J. M. Figueira, D. Abriola *et al.*, Nucl. Phys. A **787**, 484 (2007).
[57] S. B. Moraes *et al.*, Phys. Rev. C **61**, 064608 (2000).
[58] P. R. S. Gomes *et al.*, Phys. Rev. C **70**, 054605 (2004).
[59] A. R. Garcia, J. Lubian, and P. R. S. Gomes *et al.*, Nucl. Phys. A **806**, 146 (2008).
[60] C. J. Lin, J. C. Xu, H. Q. Zhang, Z. H. Liu, F. Yang, and L. X. Lu, Phys. Rev. C **63**, 064606 (2001).
[61] M. A. Tiede, D. E. Trcka, and K. W. Kemper, Phys. Rev. C **44**, 1698 (1991).
[62] M. V. Andres, J. Gomez-Camacho, and M. A. Nagarajan, Nucl. Phys. A **579**, 273 (1994).
[63] M. V. Andres, J. Gomez-Camacho, and M. A. Nagarajan, Nucl. Phys. A **583**, 817 (1995).
[64] P. A. De Young *et al.*, Phys. Rev. C **71**, 051601(R) (2005).
[65] J. P. Bychowski *et al.*, Phys. Lett. B **596**, 26 (2004).